Case Studies in Thermal Engineering 10 (2017) 169–178

Contents lists available at ScienceDirect

Case Studies in Thermal Engineering

journal homepage: www.elsevier.com/locate/csite

Experimental measurement of hermetic edge seal's thermal conductivity for the thermal transmittance prediction of triple vacuum glazing

Saim Memon

Division of Electrical and Electronic Engineering, School of Engineering, London South Bank University, 103 Borough Road, London SE17 0AA, UK

ARTICLE INFO

Keywords:
Thermal conductivity
Transient plane source
Triple vacuum glazing
Thermal performance

ABSTRACT

Thermal conductivity of hermetic edge-sealing materials plays an important part in the thermal transmittance (U-value) of the triple vacuum glazing. Thermal conductivity of Cerasolzer CS186 alloy and J-B Weld epoxy-steel resin were measured and validated with the mild-steel and indium using transient plane source method with a sensor element of double spiral and resistance thermometer in a hot disk thermal constants analyser TPS2500s are reported. The thermal conductivity data of Cerasolzer CS186 alloy and J-B Weld epoxy steel resin were measured to be 46.49 $W m^{-1} K^{-1}$ and 7.47 $W m^{-1} K^{-1}$, with the deviations (using analytical method) of ± 4% and ± 7% respectively. These values were utilised to predict the thermal transmittance value of triple vacuum glazing using 3D finite element model. The simulated results show the centre-of-glass and total U-value of 300 mm × 300 mm triple vacuum glazing to be 0.33 $W m^{-2} K^{-1}$ and 1.05 $W m^{-2} K^{-1}$, respectively. The influence of such a wide edge seal on the temperature loss spreading from the edge to the central glazing area is analysed, in which the predictions show wider edge seal has affected the centre-of-glass U-value to 0.043 $W m^{-2} K^{-1}$ due to the temperature gradient loss spread to 54 mm and 84 mm on the cold and warm side respectively.

1. Introduction

Vacuum glazing has the potential to reduce the heat loss of a building [1] and is one of the solutions proposed for the reduction of space-heating loads and carbon emissions [2]. To reduce the heat loss to a level where the U-value of the central glazing area is less than 0.5 $W m^{-2} K^{-1}$[3], the notion of triple vacuum glazing is introduced [4]. This consists of three sheets of glass, hermetic seal around the outer edge of the three glass sheets, and two evacuated gaps with a pressure below to 0.1 Pa to reduce the heat transfer by gaseous conduction and convection to a minimum level, such heat transfers can't be eliminated due to a need of an array of stainless steel support pillars, typically 0.15 mm high and 0.3 mm diameter [5], that maintain the separation of the three glass sheets. However, radiative heat transfer can be reduced by using low emittance coatings on the surfaces of the glass sheets, in this case tin-oxide coating were used.

A low temperature method of fabricating double vacuum glazing was first developed at the University of Ulster [6]. This method was based on indium or one of its alloys to seal the edges of the glass sheets hermetically at a temperature of less than 200 °C. The predicted, and experimentally determined, thermal transmittance of an indium based double vacuum glazing was reported to be less than 1 $W m^{-2} K^{-1}$ for the central glazing area [7]. In this low temperature sealing method a radiative heat transfer can be reduced to a minimum possible level by using soft low-emittance coatings on the surfaces of the glass sheets such as silver (Ag) titanium dioxide

E-mail address: S.Memon@lsbu.ac.uk.

http://dx.doi.org/10.1016/j.csite.2017.06.002
Received 29 April 2017; Received in revised form 10 June 2017; Accepted 14 June 2017
Available online 15 June 2017

Nomenclature

a	Overall radius of the sensor [m]
d	Thickness of the glass sheet [mm]
D	Dimensionless time dependent variable
k	Thermal conductivity [$W\,m^{-1}\,K^{-1}$]
P_o	Total output power from the sensor [W]
R	Resistance [ohms]
t	Time [s]
ΔT_i	Initial temperature difference [K]
$\Delta T_{ave}(\tau)$	Average temperature increase of the sample surface on the other side of the sensor [K]
T	Temperature [°C]
U	Thermal transmittance [$W\,m^{-2}\,K^{-1}$]

Abbreviations

ASTM	American Society for Testing and Materials
CALEBRE	Consumer Appealing Low Energy Technologies for Building Retrofitting
CIBSE	Chartered Institution of Building Services Engineers
FEM	Finite Element Model
TPS	Transient Plane Source
TVG	Triple Vacuum Glazing

Subscripts

ave	Average
o	Before the sensor is heated at t = 0 s
c	characteristic

Chemical formula

Ag	Silver
Al_2O_3	Aluminium oxide
In	Indium
SnO_2	Tin Oxide
TiO_2	Titanium dioxide
ZnO	Zinc oxide

Greek Letters

ρ	Density [$kg\,m^{-3}$]
α	Thermal diffusivity of the sample [$mm^2\,s^{-1}$]
τ	Dimensionless time dependent function
φ	Temperature coefficient of the resistivity [K^{-1}]
ϕ	Heat loss [W]
ε	Emittance

(TiO_2), zinc oxide (ZnO) and aluminium oxide (Al_2O_3) [6]. Due to the cost and scarcity of indium, this method has limitations for mass production. A recent low-temperature composite edge sealed triple vacuum glazing shows promising results which was first developed at Loughborough University and reported in Memon et al. (2015) [8].

In this paper the study of experimentally measuring and comparatively analysing the thermal conductivity data of the hermetic edge-seal for the thermal performance prediction are presented, because the thermal conductivity data are one of the important boundary parametric condition in the FEM of the triple vacuum glazing for which the influence of new hermetic edge seal materials on the U-value and temperature loss are analysed. It is pertinent to mention that no thermal conductivity data is supplied in the manufacturers and suppliers' datasheets for the successful application of it as hermetic edge seal materials. Some properties of Cerasolzer alloy, such as the coefficient of thermal expansion and melting temperature are provided and for J-B Weld epoxy steel resin, properties such as mechanical strength and minimum/maximum working temperatures, are available [9–11]. Fig. 1 shows the developed vacuum glazing systems facility with the modified vacuum cup for evacuation and pump-out hole sealing of the hermetic edge sealed triple vacuum glazing. The hermetic edge seal consists of the Swiss made Cerasolzer CS186 as a primary edge seal and US made J-B Weld epoxy steel resin as a secondary edge seal for the successful fabrication, by achieving a vacuum pressure of 4.8×10^{-2} Pa, in the two cavities of 500 mm × 500 mm sample of triple vacuum glazing. The primary edge seal, Cerasolzer CS186, is a composite of Sn(56%), Pb(39%), Zn(3%), Sb(1%) and Al-Ti-Si-Cu (1%) alloys [8]. This metal alloy composition was disclosed in the Japanese patent 20098/1968 [12] and is a commercial product of Asahi Glass Co., Ltd. The secondary edge sealing material used is a steel reinforced epoxy known under the commercial trade name of J-B Weld epoxy steel resin [13].

2. Methodology

A number of different instruments are available for the measurement of the thermal properties of materials [14]. There are two main methods, steady state method and transient. The steady state approach is further divided into one dimensional heat flow and radial heat flow techniques. One dimensional heat flow technique include the guarded hot plate method which is the ASTM standard based measurement system used for highly insulating materials. The radial heat flow technique includes cylindrical, spherical and ellipsoidal methods. There are a number of transient methods, which can be used for the measurement of thermal conductivity such as hot wire, transient hot strip and transient plane source methods. The experimental measurements of thermal conductivity performed in this study were undertaken using a Hot Disk thermal constants analyser TPS 2500s. This system is based on the transient plane source (TPS) method. The TPS method consists of a sensor element in the shape of a double spiral which acts both as a heat source to increase the temperature of the sample and a resistance thermometer to record the time dependent temperature increase [15]. In the current experiments, a sensor of design 7577 was used which is made of a 10 μm thick Nickel-metal double spiral. The radius of the sensor was chosen to be 2.001 mm in order to reduce the size of the sample. It is advised [16] that the diameter of the sample should not be less than twice that of the sensor diameter and the thickness of the sample should not be less than the radius of the sensor. The sensor element is usually insulated with a material to provide electrical insulation. The material used is dependent on the operating temperatures. A thin polyamide (Kapton) insulating material was chosen for the sensor insulation which is suitable

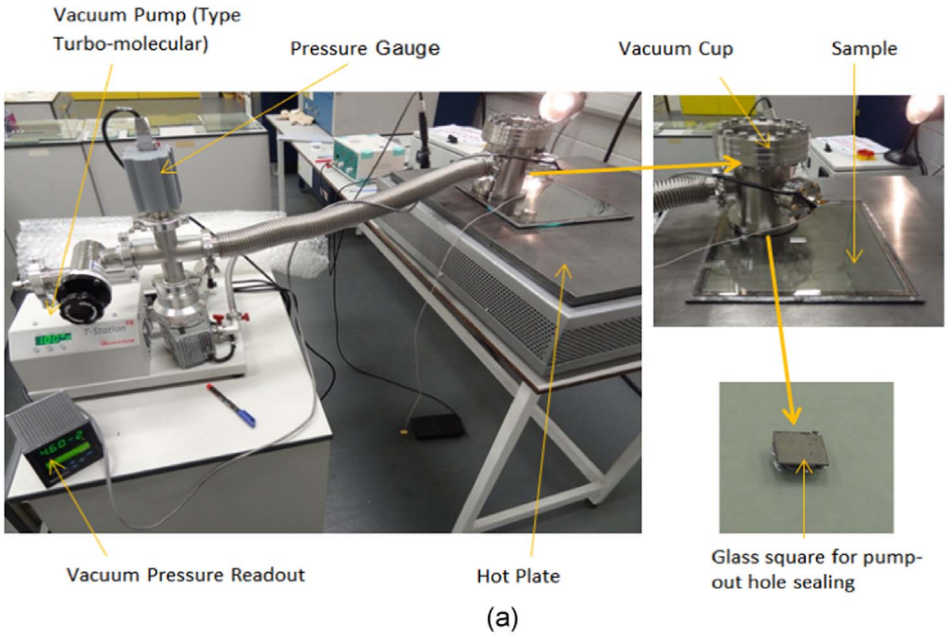

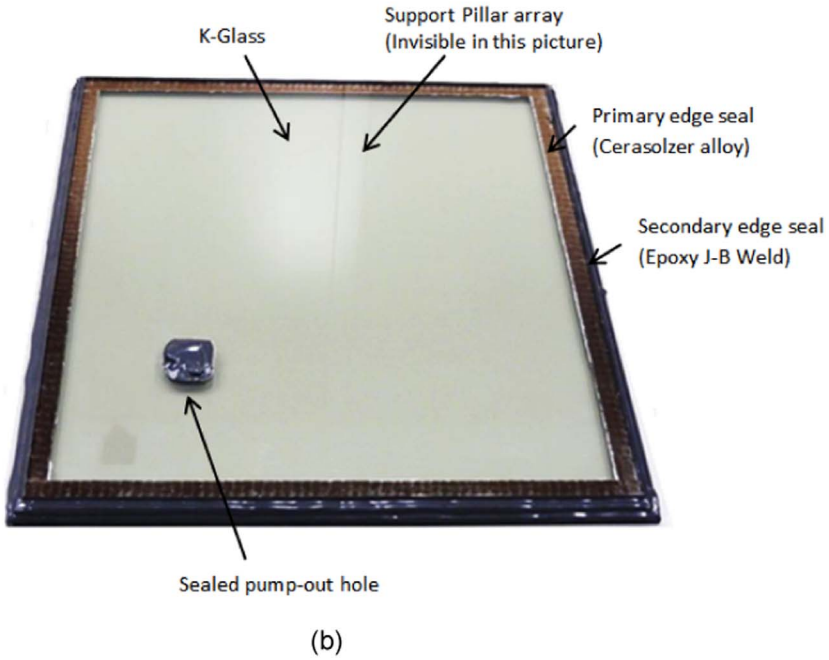

Fig. 1. (a) An illustration of the vacuum glazing production system with a modified vacuum cup for evacuation and pump-out hole sealing used for (b) the development of triple vacuum glazing.

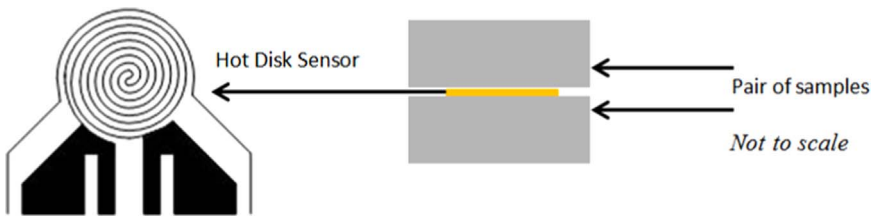

Fig. 2. A schematic diagram of the pair of samples and the Hot Disk sensor placed in between two flat cylindrical samples.

from cryogenic temperatures to about 500 K [17].

A sensor is placed between two flat cylindrical samples, as shown in Fig. 2. Passage of a constant electric power through the spiral produces heat, increases the temperature and therefore the resistance of the spiral sensor as a function of time which can be expressed according to Gustavsson et al. (1994) [14] as,

$$R(t) = R_o\{1 + \varphi[\Delta T_i + \Delta T_{ave}(\tau)]\} \tag{1}$$

Where R_o is the resistance in ohms before the sensor is heated or at time t = 0 s, φ is the temperature coefficient of the resistivity (TCR) of the sensor 7577 i.e. 46.93 × 10^{-4} K^{-1}, ΔT_i is the initial temperature difference that develops momentarily over the thin insulating layers which cover the two sides of the sensor. The thermal conductivity of the sample can be expressed according to Bohac et al. (2000) [17] as,

$$k = \frac{P_o}{\pi^{\frac{3}{2}}.\, a.\, \Delta T_{ave}(\tau)}.\, D(\tau) \tag{2}$$

Where k is the thermal conductivity of the sample in W m^{-2} K^{-1}, P_o is the total output power from the sensor in Watts, a is the overall radius of the sensor in m and $D(\tau)$ is a dimensionless time dependent function with,

$$\tau = \sqrt{\frac{t}{t_c}} \tag{3}$$

In Eq. (3), t is the time measured from the start of the transient recording and t_c is the characteristic time defined as,

$$t_c = \frac{a^2}{\alpha} \tag{4}$$

Where α is the thermal diffusivity of the sample in mm^2 s^{-1}. From the experimentally recorded temperature increase over $D(\tau)$ a straight line can be plotted which intercepts ΔT_i, and slope of $\frac{P_o}{\pi^{\frac{3}{2}}.a.\Delta T_{ave}(\tau)}$ which allows the thermal conductivity to be determined. The final straight line from which the thermal conductivity measured is obtained through a process of iteration [15]. During a pre-set time, 200 resistance recordings are taken and from these a relation between temperature and time is established.

3. Experimental setup and thermal conductivity measurement procedure

A pair of indium and Cerasolzer CS186 samples, each with a diameter of 17 mm and thickness of 3.2 mm surrounded by a hardened steel washer (to achieve uniformity of sample dimensions), were prepared, as shown in the Fig. 3. A pair of a J-B Weld epoxy steel resin samples with a diameter of 17 mm and thickness of 4 mm surrounded by a washer placed on a stainless steel plate covered with a thin layer of lithium grease, to enable separation of the samples, were also prepared as shown in the Fig. 4. All of the samples were cleaned with water and isopropanol. By using flat steel plates it was ensured that one of the surfaces of each sample was flat, this was required to avoid errors in sensor readings. The prepared sample was more than twice that of the sensor diameter (4.002 mm) and the sample thickness was more than the radius of the sensor (2.001 mm) which are the requirements advised in the instruction manual to enable precise measurements. Two test samples of cylindrical shape 30 mm in thickness and 50 mm in diameter were provided with the Hot Disk system to calibrate and verify the Hot Disk analyser's measurements. The reason an indium based sample was made is to validate the sample preparation and measuring technique using a material with well-known properties prior to determine the thermal properties of Cerasolzer alloy and epoxy J-B Weld.

The Hot Disk thermal constants analyser TPS 2500s connected to a laptop with TPS 7.0.17 version software installed must be switched on at least 60 min prior to performing an experiment to achieve thermal equilibrium within the system. The arrangement of the experimental facility is shown in the Fig. 5.

The solution of the thermal conductivity, Equ. 2, is based on the assumption that the Hot Disk sensor is located in an infinite medium and any influence from the outside boundaries of the two sample pieces sandwiching the sensor may interrupt the transient recordings. Thus a sample holder with cover, as shown in the Fig. 6, is used to minimise temperature drift before, and during, experiments. For the purpose of calibration and verification of the functioning of the analyser, a Kapton sensor type 7577 was placed

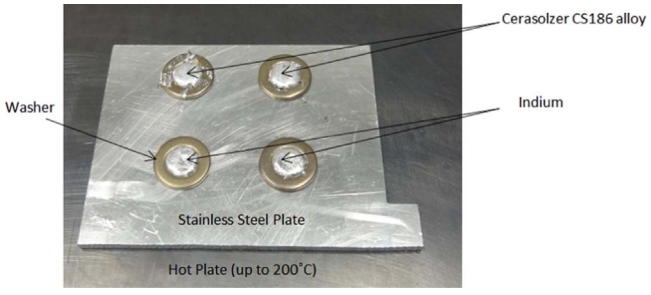

Fig. 3. A pair of indium and Cerasolzer CS186 samples with a diameter of 17 mm and a thickness of 3.2 mm surrounded by a washer produced to measure thermal conductivities using a Hot Disk thermal constants analyser.

Fig. 4. A pair of a steel reinforced epoxy J-B Weld samples with a diameter 17 mm and thickness of 4 mm surrounded by a washer produced to measure thermal conductivity using a Hot Disk thermal constants analyser.

between two mild steel calibration samples with to double spiral positioned centrally and totally covered. The two indium samples produced were characterised to confirm the sample production process. Since, the thermal conductivity of indium is well known [18]. In this paper, the repetitive thermal conductivities from four individual experiments with Cerasolzer alloy, J-B weld epoxy steel resin, Mild Steel and indium samples were undertaken to measure the average thermal conductivity of these materials.

4. Results and discussions

4.1. Experimental measurements of the thermal conductivity of the hermetic edge seal

In order to validate the measurements of Cerasolzer allow and J-B Weld epoxy the results were compared with several measurements of the samples of Mild Steel (MSteel) and Indium in four repetitive experiments, combined the cut faces flatten to reduce the experimental errors. The experimental data are plotted in Fig. 7. As can be seen this work is verified by the reported data of Mild steel and Indium. An increase of temperature with respect to reporting time interval have similar deviations and the highest increase of temperature was recorded for JB-Weld which gives a good agreement with the experimental data. The average temperature increase measured by the TPS sensor type 7577 of the mild steel, indium, J-B Weld epoxy steel resin and Cerasolzer CS186 samples are shown in Fig. 8. It can be seen that the increase in temperature in the epoxy J-B Weld is greater than the mild steel. This is due to the fact that heat flow in semi-polymeric materials is low compared to metallic materials. The temperature increase in the sample made from Cerasolzer alloy was higher than the indium sample.

An average thermal conductivity of a mild steel type SIS2343 sample was measured to be 13.76 W m^{-1} K^{-1}. The reliability of the measured thermal conductivity is compared with the standard measurement value given in the standard data sheet i.e. 13.62 W m^{-1} K^{-1}. An average thermal conductivity of the indium sample was measured to be 77.84 W m^{-1} K^{-1} with a repeatability of four times. The thermal conductivity measurement for Cerasolzer alloy and J-B Weld epoxy steel resin, as detailed in Table 1, with the deviations were calculated to be ± 4% and ± 7% in the experimental measurements as compared with the analytical methods as detailed in the Section 2.

4.2. Thermal performance analysis of hermetic edge sealed triple vacuum glazing

By utilising the measured thermal conductivities of Cerasolzer alloy as primary seal and JB- Weld as secondary seal, as detailed in

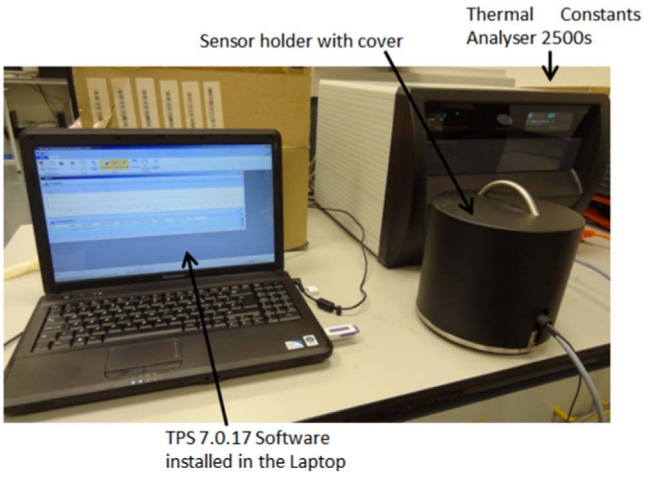

Fig. 5. Experimental setup for the measurement of thermal conductivity showing the Hot Disk thermal constants analyser connected to the laptop with TPS 7.0.17 software installed.

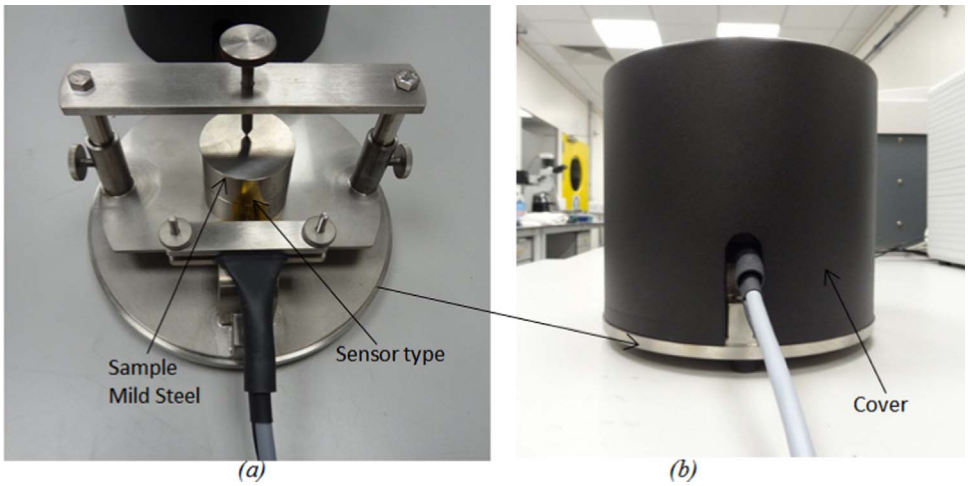

Fig. 6. Isometric view of the (a) Hot Disk Sample Holder with a Sensor positioned in between two flat cylindrical mild steel samples and (b) a side view of the Hot Disk sample holder with cover.

Table 1, a 3D FE (finite element) model based on a commercial software package MSC Marc was employed to analyse the heat transfer and predict the thermal performance of the triple vacuum glazing. The symmetry of the model was exploited to simulate the heat transfer process in computationally efficient way; only one quarter (150 mm × 150 mm) of the triple vacuum glazing of dimensions 300 mm × 300 mm was modelled and simulated using ASTM boundary conditions [19]. Three k glass sheets having thermal conductivity of 1 W m^{-1} K^{-1} with SnO_2 coatings on inner surfaces with the emissivity of 0.15 were used. The support pillars

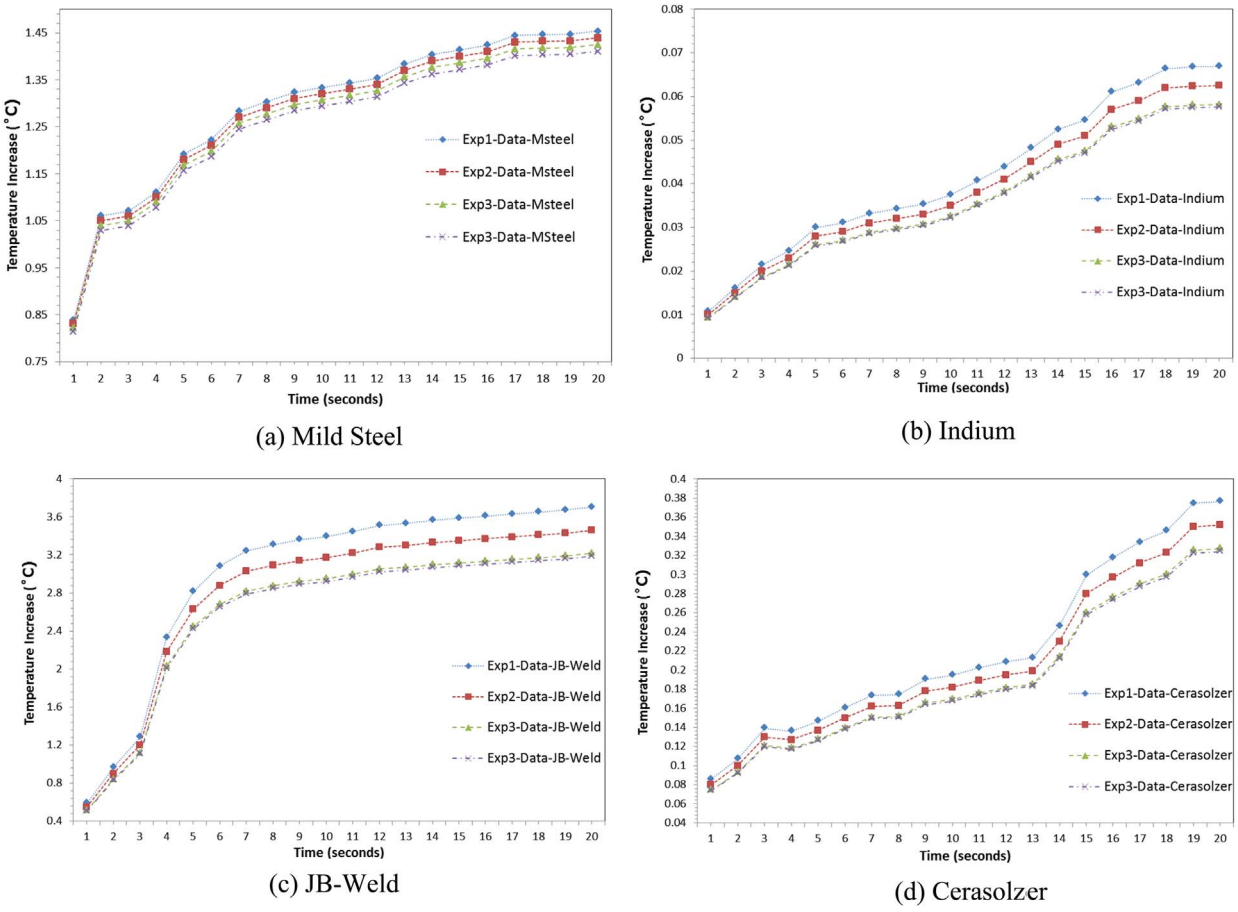

Fig. 7. Experimental results as function of temperature increase for JB-Weld and Cerasolzer in comparison to the verified Mild steel and Indium. (a) Mild Steel (b) Indium (c) JB-Weld (d) Cerasolzer.

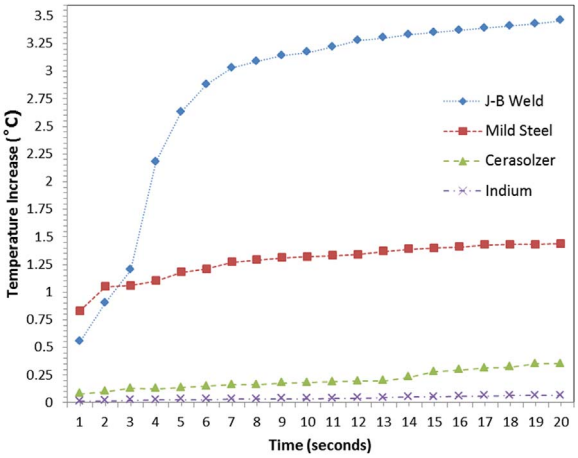

Fig. 8. The average recorded temperature increase using the TPS sensor type 7577 for the samples made from mild steel, indium, J-B Weld epoxy steel resin and Cerasolzer CS186.

were incorporated into the model explicitly [20]. This is based on the actual stainless steel pillar array having 16.2 W m^{-1} K^{-1} of thermal conductivity. The number of support pillars was employed in the triple vacuum glazing that represented by the same number of pillars in the developed finite-element model. Since modelling the pillars with circular cross-section would lead to non-uniform mesh with distorted elements around the pillar, they were modelled using square cross-section (considered the diameter of 0.3 mm. height of 0.15 mm and pillar separation of 24 mm). Additionally, it is already established in the literature that the heat transfer through the pillar does not depend upon its shape but its cross-sectional area under certain boundary conditions [21,22]. In order to keep the cross-sectional area similar to circular pillar with radius *r,* the side length of each square used is 1.78 *r*. The FE model implemented eight-node iso-parametric elements, with a total of 170455 elements and 201660 nodes to represent a quarter of the fabricated triple vacuum glazing. In FE model, the evacuated gap between glasses was represented with as a material with almost zero thermal conductivity to represent triple vacuum glazing. For sake of simplicity, the influence of residual gas among glasses was neglected in the model. In order to achieve realistic results from the simulation, a graded mesh with large number of elements was employed in the pillar. In addition to this, a convergence study was performed on the pillar to ensure the accuracy of the thermal performance predicted using the model. The material properties of the glass sheets applied to the models are those found in [18] and summarised in Table 2. The ASTM weather indoor/outdoor boundary conditions were employed in which the indoor and outdoor surface air temperatures were set to be at 21.1 °C and −17.8 °C respectively in winter conditions [19]. The internal and external surface heat transfer coefficients were set to 8.3 W m^{-2} K^{-1} and 30 W m^{-2} K^{-1} respectively [23].

The finite element 3D modelling results show a centre of glass and overall U-value of 0.33 W m^{-2} K^{-1} and 1.05 W m^{-2} K^{-1}, respectively, this is compared to the predictions of [23] i.e. 0.2 W m^{-2} K^{-1} and [5] i.e. 0.26 W m^{-2} K^{-1} as follows.

The U value (centre of glass) 0.2 W m^{-2} K^{-1}, reported by Manz et al. [23], was based on the parametric model of triple vacuum glazing without frame focused on the central glazing area. This value was achieved with 6 mm (top), 4 mm (middle) and 6 mm (bottom) thick untampered soda lime glass sheets having four layers (1-top, 2-middle and 1-bottom) of low-e coatings (ε of 0.03). It is compared with the results of this paper, it is found that an increase of U value (centre-of-glass) 0.13 W m^{-2} K^{-1}. Such deviation is due to the design of the fabricated sample reported in this paper which is made of 4 mm(top), 4 mm (middle) and 4 mm(bottom) untampered soda lime glass sheets having three layers of low-e SnO_2 coatings ($\varepsilon = 0.15$). The reason, to use such dimensions and SnO_2 coatings, is the conventional availability of glass sheets from Pilkington Glass and its use in the UK dwelling. Manz et al. (2006) has not discussed the investigations of the influence of edge effects because the simulated results were based on the parametric model focusing on the centre-of-glass area only.

The influence of edge effects is well-detailed in Fang et al. [5] and reported predicted the U values (centre-of-glass and overall) to be 0.26 W m^{-2} K^{-1} and 0.65 W m^{-2} K^{-1}, respectively. These values were reported for a TVG sample size of 500 mm × 500 mm with 4 mm (top), 4 mm(middle) and 4 mm (bottom) un-tempered soda lime glass sheets having four layers (1-top, 2-middle and 1-bottom) of low-e coatings (ε of 0.03) with a frame rebate depth of 10 mm and the width of indium-alloy edge seal 6 mm (*k* of

Table 1
Measured thermal conductivities of Cerasolzer alloy CS186 and J-B Weld epoxy steel resin and measurements of mild steel and indium.

Sample	Thermal Conductivity at 21 °C (W m^{-1} K^{-1}) [Deviation]	Measuring Time (second)	Power output from sensor [watts]
Mild Steel	13.76 [1%]	20	1
Indium	77.84 [7%]	20	1
Cerasolzer CS186	46.49 [± 4%]	20	1
J-B Weld	7.47 [± 7%]	20	1

Table 2
Parameters employed in FEM of the fabricated sample of triple vacuum glazing.

Type	Details	Value
TVG size	Top	284 by 284 by 4 mm
	Middle	292 by 292 by 4 mm
	Bottom	300 by 300 by 4 mm
Glass sheet	Thermal conductivity	1 W m^{-1} K^{-1}
Surface coating	Three low-e coatings	ε of 0.15 (SnO_2)
Glass sheet Support-Pillar	Thermal conductivity	16.2 W m^{-1} K^{-1}
	Material	Stainless steel 304
	Diameter	0.3 mm
	Height	0.15 mm
	Spacing	24 mm
Hermetic Edge Seal (Primary)	Measured thermal conductivity	46.49 W m^{-1} K^{-1}
	Material	Cerasolzer CS-186
	Width (wideness)	10 mm
Support Seal (Secondary)	Measured thermal conductivity	7.47 W m^{-1} K^{-1}
	Epoxy steel resin	J-B Weld
	Width (wideness)	4 mm

83.7 W m^{-1} K^{-1}). It can be compared, considering all factors, with the results of this paper. It is found that an increase of 0.07 W m^{-2} K^{-1} (deviation of 26.9%) and 0.4 W m^{-2} K^{-1} (deviation of 61.54%) of centre of glass and overall U value, respectively. Such deviations, as per FEM calculations, are due to: the sample size influences to a small extent as the TVG fabricated sample size was of the size 300 mm × 300 mm, the width of the edge seal influences to a large extent because the TVG fabricated sample width of edge seal used was total 14 mm (10 mm wide Cerasolzer seal and 4 mm wide J-B Weld supportive seal), the use of three SnO_2 low-e coatings (ε of 0.15) in the fabricated sample instead of four Ag low-e coatings (ε of 0.03), and there is no frame rebate depth utilised in the fabricated sample of TVG that has an influence to a small extent on the overall U value of the TVG because the purpose of this paper is focused on the hermetic sealing materials thermal conductivities and triple vacuum glazing area thermal performance only. By accounting all these factors and including the thermal conductivity of the sealing materials, the FEM model predictions are in good agreement.

The simulated isotherms of the triple vacuum glazing for the outdoor and indoor surfaces are shown in Fig. 9. The mean glass surface temperatures were simulated to be −12.55 °C and 6.71 °C for the outdoor and indoor surfaces of the total glazing area. The mean surface temperatures for the centre of glass area were simulated to be 16.43 °C and −16.60 °C for the outdoor and indoor

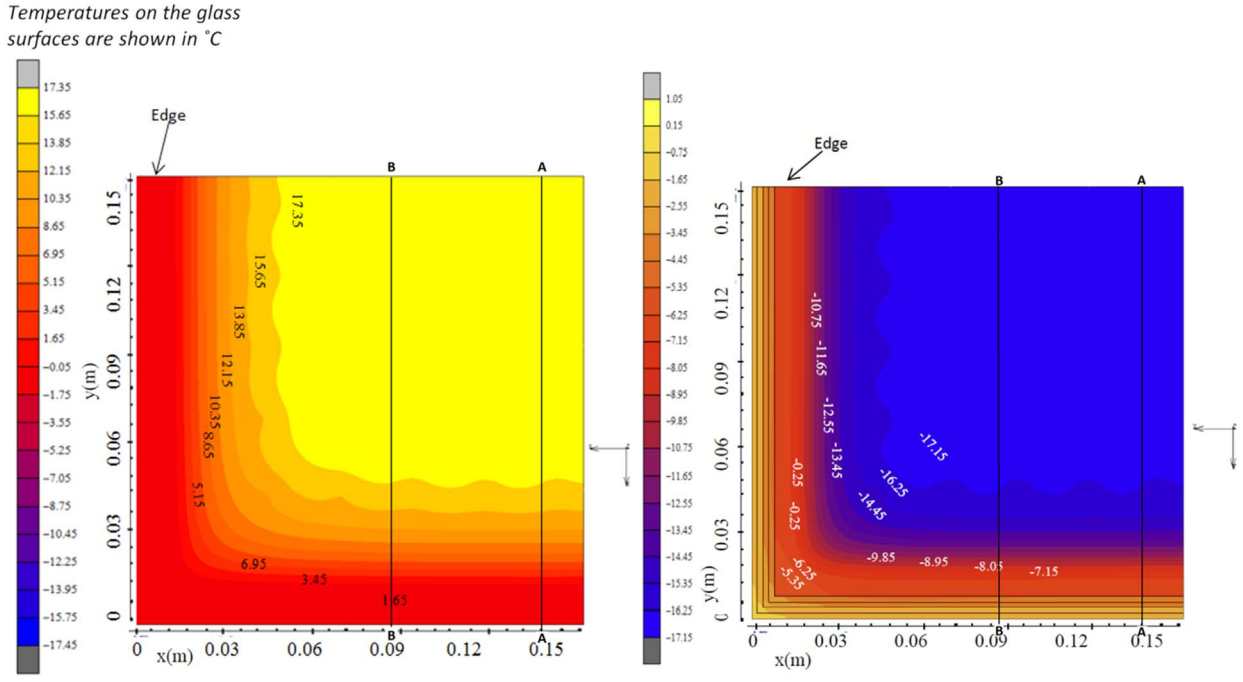

Fig. 9. The FEM based isotherms on (a) the indoor (b) the outdoor glass surface showing the temperature variations from the edge area towards the central glazing area.

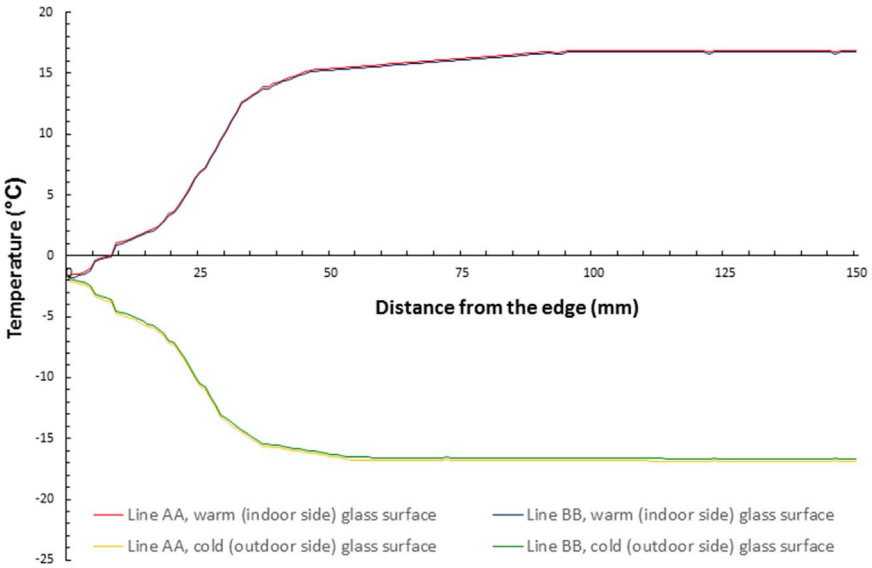

Fig. 10. The temperature loss, due to a wider edge seal, along the glazing surface lines AA and BB showing the temperature gradient from the glazing edge to the central area of the glazing of the one quarter of total sample of 300 mm x 300 mm using ASTM boundary conditions.

surfaces respectively. It can be seen the temperature discrepancies on the outdoor side are smaller than the indoor side. This is, however, due to the use of 14 mm composite edge seal as compared to the edge seal thickness of 6 mm [25]. Thus, the edge effects need to be reduced by narrowing the width of edge-seal to 9 mm (6 mm and 3 mm for primary and secondary respectively) which reduces the centre-of-glass U-value of 0.043 W m^{-2} K^{-1}.

A finite element calculations of the temperature loss due to a wider edge seal are analysed, along the outer surface lines AA and BB (as shown in Fig. 9), showing the temperature gradient from the glazing edge to the central area of the glazing as illustrated in Fig. 10. An influence of wider edge seal on temperature loss around the edge area has affected the centre-of-pane U value. Fig. 9 shows there are smaller temperature gradients on the cold surface as compared to the warm surface of the glazing which is due to the periodic shape of the edge sealing area of triple vacuum glazing as shown in Fig. 1(b). It can be seen the influence of temperature gradient loss spread to 54 mm and 84 mm on the cold and warm side respectively. When comparing with the temperature gradient profiles of [23,24] the results are in good agreement with the results presented in this paper.

5. Conclusions

In this study, a hot disk thermal constants analyser TPS 2500s using transient plane source technique with a sensor element in the shape of double spiral and resistance thermometer is proved to be an adequate in measuring and analysing the thermal conductivity of hermetic edge sealing materials (i.e. Cersolzer CS186 and J-B Weld). The technique was validated by measuring the thermal conductivity for Mild Steel and Indium and comparing these results with those available in literature. This validated technique based on hot disk thermal constants analyser was then used to measure thermal conductivity of Cerasolzer CS186 alloy and J-B Weld epoxy steel resin and found to be 46.49 W m^{-1} K^{-1} and 7.47 W m^{-1} K^{-1}, respectively. It has been shown that an increase in temperature has direct relation with respect to reporting time with highest increase in temperature was recorded for JB-Weld for a given time period, which is in agreement with the experimental data. It has also been shown that the increase in temperature in the epoxy J-B Weld is greater than that of mild steel. This observation is linked to the fact that the heat flow in semi-polymeric materials is less as compared to that of metallic materials. The temperature increase in the sample made from Cerasolzer alloy was higher than that of indium sample. These values were utilised for the numerical prediction of thermal performance of triple vacuum glazing using 3D FE model. The simulated resulted showed that the centre-of-glass and total U-value of 300mmx300mm triple vacuum glazing are 0.33 W m^{-2} K^{-1} and 1.05 W m^{-2} K^{-1}, respectively. The thermal transmittance values can be reduced by using soft low emittance coatings and by reducing the width of the hermetic edge seal to 9 mm. An influence of wider edge seal on temperature loss spreading from the edge to the central glazing area was further analysed with the FEM model calculations. In which it is concluded that the wider edge seal has affected the U-value to 0.043 W m^{-2} K^{-1} because of the temperature gradient loss spread to 54 mm and 84 mm on the cold and warm side respectively.

Acknowledgement

The author acknowledge the valuable advice and guidance received from Prof P. C. Eames during the course of this research work. This work was supported by the EPSRC funded project CALEBRE (Consumer Appealing Low energy Technologies for Building Retrofitting) [EP/G000387/1].

References

[1] S. Memon, Analysing the potential of retrofitting ultra-low heat loss triple vacuum glazed windows to an existing UK solid wall dwelling, Int. J. Renew. Energy Dev. 3 (3) (2014) 161–174.
[2] Y. Xing, N. Hewitt, P. Griffiths, Zero carbon buildings refurbishment-A Hierarchical pathway, Renew. Sustain. Energy Rev. 15 (2011) 3229–3236.
[3] P. Eames, Vacuum glazing: current performance and future prospects, Vacuum 82 (2008) 717–722.
[4] W. Wuethrich, Heat transmission reducing closure element, European Patent No. 1529921, 2005.
[5] Y. Fang, T.J. Hyde, N. Hewitt, Predicted thermal performance of triple vacuum glazing, Sol. Energy 84 (12) (2010) 2132–2139.
[6] P.W. Griffiths, P.C. Eames, T.J. Hyde, Y. Fang, B. Norton, Experimental characterization and detailed performance prediction of a vacuum glazing system fabricated with a low temperature metal edge seal, using a validated computer model, ASME J. Sol. Energy Eng. 128 (2006) 199–203.
[7] J.F. Zhao, P.C. Eames, T.J. Hyde, Y. Fang, J. Wang, A modified pump-out technique used for fabrication of low temperature metal sealed vacuum glazing, Sol. Energy 81 (2007) 1072–1077.
[8] S. Memon, F. Farukh, P.C. Eames, V.V. Silberschmidt, A new low-temperature hermetic composite edge seal for the fabrication of triple vacuum glazing, Vacuum 120 (2015) 73–82.
[9] Senju Metal Industry Co., Ltd. Cerasolzer #C186-material safety data sheet. Senju Metal Industry Co. Ltd., Tokyo, 2013.
[10] H. Yamamoto, R. Ohmuro, Imaging device utilizing solid-state image sensors combined with a beam-splitting prism, US Patent publication No. 4,916,529, Japan, 1990.
[11] Asahi Glass Co., Ltd., Cerasolzer New Metal Solder for Glass and Ceramics, 1991.
[12] MBR Electronics GmbH, Cerasolzer product information. [Viewed on 03/12/16] Available from 〈http://cerasolzer.com/cerasolzer/basic_info_gb.html〉.
[13] J.-.B. Weld, J-B Weld adhesive resign and hardener. [Viewed on 06/05/16] 〈http://www.jb-weld.co.uk/technical-data-sheets〉.
[14] M. Gustavsson, E. Karawacki, S.E. Gustafsson, Thermal conductivity, thermal diffusivity, and specific heat of thin samples from transient measurements with hot disk sensors, AIP Publishing LLC, Rev. Sci. Instrum. 65 (1995) 3856.
[15] S.E. Gustavsson, Transient plane source techniques for thermal conductivity and thermal diffusivity measurements of solid materials, AIP Publishing LLC, Rev. Sci. Instrum. 62 (1991) 797.
[16] Hot Disk Thermal Constants Analyzer, TPS 2500s Instruction Manual, Mathis Instruments. [Viewed on 05/07/2013], 2013.
[17] V. Bohac, M.K. Gustavsson, L. Kubicar, S.E. Gustafsson, Parameter estimations for measurements of thermal transport properties with the hot disk thermal constants analyser, AIP Publishing LLC, Rev. Sci. Instrum. 71 (2000) 2452.
[18] Indium. Physical constants of pure indium. Indium Corporation.[Viewed on 25/08/2016] Available from 〈http://www.indium.com/metals/indium/physical-constants/〉.
[19] ASTM., Standard procedures for determining the steady state thermal transmittance of fenestration systems, ASTM Standard E 1423-91, in: 1994 Annual Book of ASTM Standard 04.07, American Society of Testing and Materials, 1991, pp. 1160–1165.
[20] S. Memon, Design, fabrication and performance analysis of vacuum glazing units fabricated with low and high temperature hermetic glass edge sealing materials, Ph.D. Thesis Loughborough University Institutional Repository, UK, 2013 (DOI), 〈https://dspace.lboro.ac.uk/2134/14562〉.
[21] R.E. Collins, S.J. Robinson, Evacuated glazing, Sol. Energy 47 (1) (1991) 27–38.
[22] J. Wang, P.C. Eames, J.F. Zhao, T. Hyde, Y. Fang, Stresses in vacuum glazing fabricated at low temperature, Sol. Energy Mater. Sol. Cells 91 (2007) 293–303.
[23] Y. Fang, T.J. Hyde, N. Hewitt, P.C. Eames, B. Norton, Comparison of vacuum glazing thermal performance predicted using two and three dimensional models and their experimental validation, Sol. Energy Mater. Sol. Cells 93 (2009) 1492–1498.
[24] H. Manz, S. Brunner, L. Wullschleger, Triple vacuum glazing: heat transfer and basic mechanical design constraints, Sol. Energy 80 (2006) 1632–1642.
[25] Y. Fang, T.J. Hyde, F. Arya, N. Hewitt, R. Wang, Y. Dai, Enhancing the thermal performance of triple vacuum glazing with low-emittance coatings, Energy Build. 97 (2015) 186–195.